Ann. Geophys., 28, 203–215, 2010
www.ann-geophys.net/28/203/2010/

Annales Geophysicae

On the 3-D reconstruction of Coronal Mass Ejections using coronagraph data

M. Mierla[1,2], B. Inhester[3], A. Antunes[4], Y. Boursier[5,6], J. P. Byrne[7], R. Colaninno[8], J. Davila[9], C. A. de Koning[10], P. T. Gallagher[7], S. Gissot[2], R. A. Howard[4], T. A. Howard[11,12], M. Kramar[13], P. Lamy[5], P. C. Liewer[14], S. Maloney[7], C. Marqué[2], R. T. J. McAteer[7], T. Moran[9], L. Rodriguez[2], N. Srivastava[15], O. C. St.Cyr[9], G. Stenborg[16], M. Temmer[17], A. Thernisien[18], A. Vourlidas[4], M. J. West[2], B. E. Wood[4], and A. N. Zhukov[2,19]

[1]Institute of Geodynamics of the Romanian Academy, Bucharest, Romania
[2]Solar-Terrestrial Center of Excellence – SIDC, Royal Observatory of Belgium, Brussels, Belgium
[3]Max-Planck-Institut für Sonnensystemforschung, Katlenburg-Lindau, Germany
[4]Naval Research Laboratory, Washington, D.C., USA
[5]Laboratoire d'Astrophysique de Marseille, Marseille, France
[6]Signal Processing Institute, EPFL, Lausanne, Switzerland
[7]Astrophysics Research Group, School of Physics, Trinity College Dublin, Dublin 2, Ireland
[8]George Mason University, Fairfax, USA
[9]NASA – Goddard Space Flight Center, MD, USA
[10]CIRES-SWPC, University of Colorado, Boulder, CO, USA
[11]Air Force Research Laboratory, National Solar Observatory, Sunspot, NM 88349, USA
[12]Department of Space Studies, Southwest Research Institute, Boulder, CO 80302, USA
[13]Catholic University of America, Washington D.C., USA
[14]Jet Propulsion Laboratory, California Institute of Technology, Pasadena, CA 91109, USA
[15]Udaipur Solar Observatory, Physical Research Laboratory, Udaipur, India
[16]Interferometrics, Inc., Herndon, USA
[17]Kanzelhöhe Observatory/IGAM, Institute of Physics, University of Graz, Graz, Austria
[18]Universities of Space Research Association, Columbia, MD, USA
[19]Skobeltsyn Institute of Nuclear Physics, Moscow State University, Moscow, Russia

Received: 13 June 2009 – Revised: 4 January 2010 – Accepted: 12 January 2010 – Published: 20 January 2010

Abstract. Coronal Mass ejections (CMEs) are enormous eruptions of magnetized plasma expelled from the Sun into the interplanetary space, over the course of hours to days. They can create major disturbances in the interplanetary medium and trigger severe magnetic storms when they collide with the Earth's magnetosphere. It is important to know their real speed, propagation direction and 3-D configuration in order to accurately predict their arrival time at the Earth. Using data from the SECCHI coronagraphs onboard the STEREO mission, which was launched in October 2006, we can infer the propagation direction and the 3-D structure of such events. In this review, we first describe different techniques that were used to model the 3-D configuration of CMEs in the coronagraph field of view (up to 15 $R_{\odot}$). Then, we apply these techniques to different CMEs observed by various coronagraphs. A comparison of results obtained from the application of different reconstruction algorithms is presented and discussed.

Keywords. Solar physics, astrophysics, and astronomy (Flares and mass ejections)

Correspondence to: M. Mierla
(mmierla@gmail.com)

1 Introduction

Coronal mass ejections (CMEs) are transient events where coronal plasma is ejected by the Sun at velocities ranging from less than 200 km s^{-1} to more than 2000 km s^{-1} (e.g. Yurchyshyn et al., 2005). They play an important role for space weather, as they can induce severe magnetic storms when they interact with the Earth's magnetosphere. Generally speaking, fast moving halo CMEs (i.e. fast CMEs with

an apparent width of around 360° in a coronagraph field of view) directed towards the Earth have been known to produce strong geomagnetic storms (Gosling et al., 1990; Srivastava and Venkatakrishnan, 2002, 2004). Not only halo CMEs but also occasionally limb CMEs may result in strong geomagnetic storms (Schwenn et al., 2005; Gopalswamy et al., 2010). In addition to the speed of the CME, the magnetic field orientation of the interplanetary CME (ICME) also plays an important role. When the magnetic field in the ICME is strong, southward and long-lasting, a strong geomagnetic storm is likely to occur (Russell et al., 1974; Gonzalez and Tsurutani, 1987). Ruzmaikin et al. (2003) and Yurchyshyn et al. (2003) suggested that the magnetic field orientation of the erupting filaments associated with the CMEs and the associated magnetic clouds are related. Therefore it is important to have an accurate estimation, not only of the speed and direction of the CME propagation, but also of the three-dimensional (3-D) geometry.

CMEs are typically observed in white light images provided by space-based coronagraphs such as LASCO (Brueckner et al., 1995) and ground-based instruments such as the MK III and MK IV coronagraphs at Mauna Loa. Coronagraphs provide us with a two-dimensional representation of the CME three-dimensional structure projected onto the plane of the sky (POS). As a consequence, the measured quantities like angular width, height, speed as well as derived quantities like mass and energy of CMEs are also projected on this plane and therefore, represent lower limits of the true, un-projected CME properties. The projection effects on these quantities can be estimated by making assumptions about the CME propagation direction and shape, but the true 3-D properties of the CME remain difficult to estimate reliably (Vršnak et al., 2007). The new data from the Solar TErrestrial RElations Observatory (STEREO) (Kaiser et al., 2008), which was launched in October 2006, provides us with stereoscopic images of the Sun's atmosphere. The two STEREO spacecraft orbit the Sun at approximately 1 AU near the ecliptic plane with a separation angle between them increasing at a rate of about 45 degrees/year. The first satellite orbits Ahead of the Earth in it's orbit around the Sun, and the second Behind (labeled A and B, respectively, hereon). The stereoscopic images obtained by the Sun Earth Connection Coronal and Heliospheric Investigation (SECCHI) instrument suite (Howard et al., 2008) aboard STEREO allow us to make 3-D estimations of the structure and kinematic parameters of CMEs.

1.1 Constraints in reconstructing the CMEs

Several attempts at reconstructing the 3-D structure of CMEs had been made prior to the launch of STEREO. These include the use of polarization brightness measurements (Munro, 1977) from as long ago as the Skylab coronagraph era. These methods were re-explored using more recent data sets and analysis by Moran and Davila (2004) and Dere et al. (2005). When observed from a single vantage point such as the SoHO spacecraft, 3-D reconstruction may only be attempted considering a simple geometry which maintains quasi similarity over the entire sequence of images. With such a method, an initial parametric description of the 3-D distribution of electrons is required, and forward modeling (FM) is performed to generate a set of synthetic images which are compared to the observed ones. Trial and error adjustments of the parameters then produce the best fit characterizing the CME (e.g. Chen et al., 1997; Thernisien et al., 2006). The expectation was that stereoscopic observations from the two STEREO spacecraft would provide enough information to estimate the 3-D characteristics of CMEs. However, it has been found that in most cases two views are still not enough for the 3-D reconstruction of CMEs. Hence we still have to rely on assumptions and a priori constraints when trying to resolve the CME shape, although these assumptions may be less demanding than compared to the single view case, and the parameters fitted to the two images to define the CME shape are more reliable. Some of the main problems in reconstructing CMEs are: 1) the complexity of CME phenomena; 2) the difficulty in identifying the same feature in the images used for reconstruction.

The first problem is the complexity of the CME phenomena. Generally, the coronagraph images reveal a very large variety of apparent morphologies (from bubble-like shape to more complex structures like flux-ropes etc.). Figure 1 is a good example of a "three-part" CME, consisting of a bright circular front, followed by a dark cavity and a bright compact core (Illing and Hundhausen, 1986). CMEs are also highly dynamic events and their global appearance may change considerably in successive images (see Fig. 1).

Another problem is the correct identification and matching of features of a CME in stereo images for reconstruction purpose. The problem lies in correctly identifying the projections of an object/feature in the two stereo images. While it is usually possible to identify the CME in two images and thus determine its general 3-D location, it is not easy to identify features within the CME. To establish a relationship between the projections (so called correspondence) is one of the key problems of stereoscopic reconstructions (e.g. Inhester, 2006). Generally, the methods to find correspondences between the stereo images used in classical stereoscopy are classified in correlation- and feature-based approaches (e.g. Trucco and Verri, 1998). If well defined shapes can be identified in the two images then a feature-based approach can be used. This may work for small scale blobs, sharp corners or kinks often displayed by the dense filament material inside CMEs. Unfortunately, the outer boundaries of CMEs often have a rather diffuse density distribution where prominently located points are difficult to identify. In such cases correlation-based correspondences appear more promising. However, even if the outer boundary is marked by a smooth circular surface with a steep density gradient, its reconstruction is hampered by the fact that,

depending on the STEREO base angle, the visible leading edges (LE) in the two STEREO images tangentially project two different sections of the CME surface. The effect on the triangulation of the CME surface can be estimated and compensated if a curvature radius of the CME surface in the respective epipolar plane is assumed.

The attempts to reconstruct the CME shape are further complicated because the CME plasma is optically thin and its observed radiance results from the integration of the Thomson scattering by coronal electrons along the line of sight (LOS). This allows the possibility that overlapping structures will create a sharp bright boundary from one viewpoint but show a more diffuse complex structure from the other, thus complicating the proper identification of CME boundaries or fine structure.

If one can overcome the above mentioned difficulties, and a one to one pixel correspondence can be found in the two images, then the reconstruction is a purely linear geometrical task for individual tie-points (TP). For extended objects with unknown shapes, the problem of reconstruction from a fewer number of view directions, is heavily underdetermined. There are multiple possible solutions for underconstrained problems, each of which can reproduce the observed data. Therefore additional constraints have to be evoked to render the reconstruction a uniquely solvable problem. The problem depends on the desired complexity of the solution i.e. on the number of parameters that need to be retrieved from observations. As discussed above, CME shapes are complex, making approximate and smoothed models a good compromise, but in some cases assumptions about the shape of the model are still required. By reducing the model parameters, we also reduce the amount of useful data obtained from the model, to the point where we can only extract the propagation direction and CME speed. Generally, fewer parameters require less a priori assumptions, and the results are more robust. Depending on the constraints added for each technique, one may get different reconstruction results. When evaluating the results, it is therefore vital to keep the assumptions made in mind.

The purpose of this paper is to illustrate different techniques which have been used to infer 3-D properties of CMEs measured by coronagraphs and to compare the results obtained by applying these techniques to current data (mostly SECCHI-COR on STEREO and LASCO on SOHO).

We do not include here the extensive and different analysis techniques applied to CMEs in the heliosphere (e.g. Jackson and Hick, 2005; Jackson et al., 2006, 2008; Tappin and Howard, 2009; Tokumaru et al., 2007) using Helios, Solar Mass Ejection Imager (SMEI) and interplanetary scintillation (IPS) observations. Such analysis techniques generally fit observations of CMEs in the interplanetary medium by using their outward expansion to gain perspective views to study their propagation and mass, and do so at a resolution far below that of the initial image data.

2 Reconstruction techniques

Several techniques have been developed to infer the location of coronal structures in 3-D space (Pizzo and Biesecker, 2004; Inhester, 2006; Feng et al., 2007; Aschwanden et al., 2008; Rodriguez et al., 2009). Previous geometric parameters of halo CMEs have been measured by using a cone model technique applied to LASCO data (e.g. Zhao et al., 2002; Michalek et al., 2003; Xie et al., 2004; Krall et al., 2006; Michalek, 2006). Their assumption is based on the fact that CMEs propagate almost radially beyond 2 $R_{\odot}$ with nearly constant angular widths. The flux-rope shaped CMEs have been modeled by Chen et al. (1997); Gibson and Low (1998); Chen et al. (2000); Wu et al. (2001); Manchester et al. (2004); Krall (2007); Thernisien et al. (2009) and cloud-like CMEs by Boursier and Lamy (2010). In another study, Cremades and Bothmer (2004) derived the geometrical properties of structured CMEs from a set of 124 flux rope CMEs observed in LASCO-C2 data. Based on this study, Thernisien et al. (2006) developed a forward-modeling technique for flux-rope-like CMEs in order to reproduce the CMEs morphology. Another technique that has been used to infer the three-dimensional structure of a CME makes use of polarization measurements of the white-light corona (Moran and Davila, 2004; Dere et al., 2005).

With the launch of the STEREO spacecraft, new techniques are now being evaluated to derive the direction of propagation of CMEs and as a consequence their propagation speeds in a 3-D coordinate system (e.g. Mierla et al., 2008; Howard and Tappin, 2008; Boursier et al., 2009; Colaninno and Vourlidas, 2009; de Koning et al., 2009; Srivastava et al., 2009; Temmer et al., 2009). Attempts to infer the 3-D structure have also been done by several authors (e.g. Antunes et al., 2009; Mierla et al., 2009; Moran et al., 2010; Thernisien et al., 2009; Wood et al., 2009); however, as pointed out earlier many assumptions need to be considered in order to get a unique solution. One such assumption is that CMEs expand radially and in a self-similar fashion as they propagate outwards (e.g. Thernisien et al., 2009; Wood et al., 2009). Another assumption is that affine geometry holds valid in the coronagraph field of view and should be used instead of projective geometry (e.g. Liewer et al., 2009b; Mierla et al., 2008; Srivastava et al., 2009). The use of affine geometry is justified since the objects that are to be reconstructed are typically 200 $R_{\odot}$ away from the observer. This distance is much greater than the typical size of the objects/features and their distance from the Sun. Affine geometry assumes the observer is located at an infinite distance, such that different viewing angles can be considered parallel, and objects near the Sun appear the same size independent of their distance, h, from the plane of the sky. In the case of projective geometry, the finite distance of the STEREO spacecraft at 200 $R_{\odot}$ compared to distance, h, is taken into account. If the CME is propagating towards one of the STEREO spacecraft, its size in the image will appear enlarged by a factor

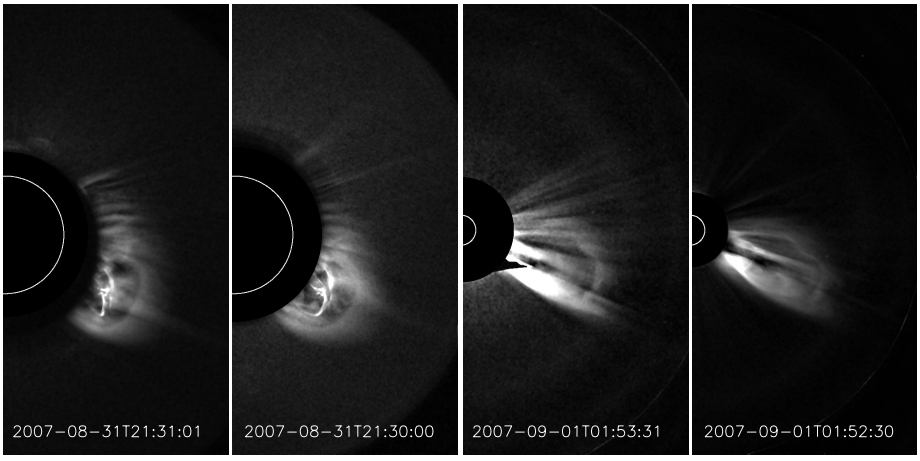

Fig. 1. The CME on 31 August–1 September 2007 observed by SECCHI-COR1 (the left two columns) and by SECCHI-COR2 (the right two columns) coronagraphs. Both A (second and fourth columns) and B (first and third columns) spacecraft images are shown. COR1 images show the white light total brightness corona from 1.4 to 4 $R_{\odot}$. COR2 images show the white light total brightness corona from 2.5 to 15 $R_{\odot}$. In all panels the visible solar disc is represented by the white circle, while the larger dark disc shows the coronagraph occulter. The images were co-aligned in the STEREO mission plane. Adapted from Mierla et al. (2009).

$1/(1-h/200\,R_{\odot})$. Therefore assuming affine geometry, one would overestimate its size by this factor.

We assessed several methods that have been used by different authors for three-dimensional representation of CMEs. These are listed in Table 1, and will be further described below.

2.1 Epipolar geometry and Tie point (TP) reconstruction

The most used method of reconstructing CMEs in coronagraph data is tie-pointing (TP); closely related to tie pointing is triangulation (Tr) (Liewer et al., 2009a).

In order to apply the reconstruction technique for STEREO observations, the positions of the two spacecraft can be considered as two view points or two observers. The positions of the two STEREO spacecraft and the point in the solar corona to be triangulated define a plane called the epipolar plane (e.g. Inhester, 2006). Since every epipolar plane is seen head-on from both spacecraft, it is reduced to a line in the respective image projections. This line is called epipolar line. Any object identified to be situated on a certain epipolar line in one image must lie on the same epipolar line in the other image. Finding a correspondence between pixels in the images taken by spacecraft A and B is therefore reduced to establish such a correspondence along the same epipolar lines in both images. Finding the correspondence can be done by eye (by tracking conspicuous features of the leading edge, like density variations, prominently shaped structures or localized blobs of plasma) or automatically using a local correlation tracking (LCT) method. In the LCT method, a cross correlation is calculated between the intensity of the two stereo images along common epipolar lines. The maximum of the correlation, as a function of the relative shift along the epipolar line, is taken as evidence for a local correspondence.

Once the correspondence between the pixels is found, the 3-D reconstruction is achieved by calculating the lines of sight that belong to the respective pixels in the image and tracking them back into the 3-D space. Since the lines of sight have to lie in the same epipolar plane, their intersection in this plane is unambiguously defined. This procedure is often called tie-pointing (e.g. Inhester, 2006).

There are several derivatives of this method: the 3-D height-time technique (3D-HT) (see Mierla et al., 2008; Maloney et al., 2009), local correlation tracking (to identify the same feature in A and B images), plus the triangulation technique (LCT-TP) (Mierla et al., 2009); triangulation using the combination of two or three spacecraft (STEREO or STEREO + SOHO) (de Koning et al., 2009; Temmer et al., 2009). The most common feature reconstructed by TP is the leading edge (LE) of a CME (de Koning et al., 2009; Liewer et al., 2009b; Srivastava, 2009; Srivastava et al., 2009; Temmer et al., 2009) and more compact structures, such as the core of the CME (Mierla et al., 2008). Also, triangulation of the center of gravity (CoG) or the center of mass (CM) in each image is performed, where this location is assumed to represent the global position of the CME in 3-D (Boursier et al., 2009; de Koning et al., 2009; Mierla et al., 2009).

2.2 Forward modeling and inverse reconstruction

Forward modeling assumes a specific parametric shape and iteratively fits the model until it produces renderings that

Table 1. Reconstruction techniques. See text for the abbreviations of sub-techniques.
.

Name of the technique	Sub-technique	References	Comments
Forward modeling (FM)	flux-rope model	Thernisien et al. (2006)	one view direction.
		Wood et al. (2009)	a priori known shape.
	hemispherical shell	Boursier et al. (2009)	
Tie-pointing plus triangulation (TP-Tr)	CoG+Tr	Boursier et al. (2009)	at least two view directions. correct identification of the same feature in A and B images, required.
	Tr	de Koning et al. (2009)	
	Tr	Howard and Tappin (2008)	
	Tp-Tr	Liewer et al. (2009a)	
	3D-HT	Mierla et al. (2008)	
	3D-HT	Srivastava (2009)	
	LCT+TP	Mierla et al. (2009)	
	CM+TP	Mierla et al. (2009)	
	TP-Tr	Srivastava et al. (2009)	
	Tr	Temmer et al. (2009)	
Constraint on the Mass Calculation (MassConstr)	Thomson scattering based	Colaninno and Vourlidas 2009	the same mass in A and B images.
Inverse reconstruction plus forward modeling (InvRec+FM)	flux rope plus inverse modeling	Antunes et al. (2009)	at least two view directions. requires large STEREO separation.
Polarization ratio (PR)	Thomson scattering based	Moran et al. (2010)	one view direction.
		Mierla et al. (2009)	

match the actual data. Forward modeling produces a physical solution based on model assumptions, but predisposes that the solution only fits that model. Inverse modeling is a non-parametric method that assumes no pre-defined shape for the CME and uses grid minimization to solve for an underlying 3-D electron density distribution by comparing renderings with the actual data views taken. In contrast to forward modeling, inverse modeling usually produces non-unique solutions. In essence, inverse modeling is underconstrained and forward modeling is overconstrained. Antunes et al. (2009) have used a hybrid method by combining inversion with forward modeling in order to infer the 3-D structure of CMEs recorded by STEREO. The authors used the PIXON method to reconstruct this density distribution, which is based on minimizing the number of electron density volumetric elements necessary to reproduce the observations. The PIXON method is described in Puetter et al. (2005).

Forward modeling relies on physical models of CME magnetic structures. Many of these models assume that a magnetic flux rope topology is at the core of all CMEs. Thernisien et al. (2009) have applied the Graduated Cylindrical Shell (GCS) model on CME events observed by the SECCHI/COR2 A and B instruments. The GCS model is meant to reproduce the large scale structure of flux rope-like CMEs. It consists of a tubular section forming the main body of the structure attached to two cones that correspond to the "legs" of the CME. The electrons are placed only at the surface and the prominence material is not modeled.

Wood et al. (2009) attempted to reconstruct the 3-D mass distribution of a CME using a trial-and-error method, where synthetic SECCHI images were computed from an assumed 3-D density distribution, and then the distribution was repeatedly altered to obtain better visual agreement with the data.

Boursier et al. (2009) reconstructed the leading surface of a CME using a hemispherical shell. For that purpose the authors reduced the problem into a minimization problem where they constrained the lines of sight corresponding to points on the apparent leading edge on images to be tangent to the spherical shell to be reconstructed.

2.3 Techniques based on Thomson scattering properties

It is known that the visible emission of the K-corona originates from the scattering of photospheric light by the coronal electrons (Minnaert, 1930; Van de Hulst, 1950; Billings, 1966) via the Thomson scattering mechanism (Jackson, 1997). Here we present different techniques that use this effect to reconstruct 3-D objects.

2.3.1 Polarization ratio technique (PR)

The degree of polarization of Thomson-scattered light by coronal electrons is a function of the scattering angle

between the direction of the incident light and the direction towards the observer (χ) (Billings, 1966). This effect allows estimation of an effective scattering angle from the ratio of polarized to unpolarized brightness which determines an effective distance of the scattering location from the plane of the sky. If one can resolve the front-to-back ambiguity of the polarization, the PR technique can be employed to obtain a 3-D reconstruction of a CME from coronagraph images obtained with different polarizer orientations (Moran and Davila, 2004; Dere et al., 2005). It should be noted that the PR method is applied separately to COR-A and COR-B images. By applying the method to both sets of images we get two different answers that can be compared with each other, thus also giving an idea about the method uncertainty.

2.3.2 Constraint on the mass calculation (MassConstr)

The observed intensity of a CME depends on ϕ, which is the angle the electrons make with the POS. From intensity images, Colaninno and Vourlidas (2009) calculated the electron density and mass for various values of ϕ. A simple requirement is that the total mass of a CME remains the same when the mass calculation is corrected for the two viewpoints. In doing so, it is possible to simultaneously derive the direction and total mass of the CME (Colaninno and Vourlidas, 2009).

3 Observations and data processing

White-light coronagraph images recorded with SECCHI-COR instruments are mainly used for 3-D reconstruction of CMEs. The SECCHI-COR1 coronagraph is a classic Lyot internally-occulted coronagraph which observes the white light corona from 1.4 to 4 $R_\odot$ (Thompson et al., 2003; Thompson and Reginald, 2008). SECCHI-COR2 is an externally occulted Lyot coronagraph which observes the coronal emission in visible light from 2.5 to 15 $R_\odot$. The COR1 and COR2 coronagraphs include a linear polarizer which is used to suppress scattered light and to extract the polarized brightness signal from the solar corona. The total brightness and polarized brightness is extracted from three sequential images taken with polarization angles of 0°, 120° and 240°. Here we also consider the white light images taken by LASCO-C2 and C3 coronagraphs onboard SOHO which have a field of view from 2 to 6 $R_\odot$ and from 3.7 to 32 $R_\odot$, respectively.

CMEs are faint when observed against the background F- and K-corona emission, so further processing is necessary to extract and enhance the CME relative to the background. First, the standard SECCHI_PREP routine provided by the SECCHI team is applied for basic instrumental corrections. Then, different background images are subtracted depending on the purpose of the study. For space weather forecasters who use geometric localization, subtraction of a pre-event image is sufficient. In the case of exceptionally faint events, especially when used for research applications, this process is not sufficient to visualize the CME and further image processing techniques such as filtering (wavelet, radial gradient etc.) are applied. In the case of polarimetric analysis, a pre-event image, or an event minimum background is subtracted in order to obtain Thomson scattered emission solely from the CME. The event minimum image is obtained by computing the minimum value in each pixel, from a set of images obtained over a period of several hours, ranging a few hours either side of the time when the CME was observed. Figure 1 shows an example of a CME on 31 August–1 September 2007, which was observed in both COR1 (left two panels) and COR2 (right two panels) instruments from which an event minimum background was subtracted. The images were also smoothed by a 5×5 pixel median filter.

The reconstruction results for all the CMEs presented in this paper have been calculated in the same coordinate system, i.e. the Heliocentric Earth Equatorial (HEEQ) coordinate system. The HEEQ coordinate system has its origin at the Sun's center, the Z-coordinate axis along the solar rotation axis and the X-axis so that Earth lies in the X-Z plane. The Stonyhurst heliographic coordinates which are closely related to HEEQ coordinates were also used (e.g. Thompson, 2006). The new coordinates are represented in a spherical coordinate system as latitude, longitude and distance from the Sun's center. The value of the longitude ranges between $-180°$ and $+180°$. This also implies that the front-side disk longitude ranges between $-90°$ and $+90°$. The image coordinates are given by the x-axis (the horizontal axis) and the y-axis (the vertical axis).

4 Application of the reconstruction techniques

The results obtained by applying the methods described in Sect. 2 to different CMEs are shown in Table 2. The time of each CME is recorded when observed in the COR1 field of view. Each event is briefly described below.

4.1 15 May 2007 CME

A CME was observed at 19:00 UT on 15 May 2007. The source active region of this CME was located at N02E47. The orientation of the neutral line was approximately along the north-south direction. The separation angle of the two STEREO spacecraft was 8°. By applying the three aforementioned methods (LCT-TP, CM-TP and PR) to this event Mierla et al. (2009) have derived the propagation direction of the CME, and the results are shown in Table 2. The estimated latitudes and longitudes show remarkable agreement, where the longitudes of the reconstructed points differ up to 20° and the latitudes up to 10° when compared with the source region on the disk. This deviation could be due to a deflection of the CME from its radial direction (St. Cyr et al., 1999). Temmer et al. (2009) used both STEREO and

Table 2. Values of parameters for different events reconstructed using different methods applied on COR and LASCO data. The errors for different methods are estimated as described in Sect. 5.1. ⋆ means that identifying the same feature in all spacecraft is required and ⋆⋆ means that the entire CME should be seen in all spacecraft for the methods to work. The time of each CME is recorded when observed in the COR1 FOV.

Date	γ°	Author	Method	Lat	Lon	Speed km s^{-1}	Remarks
			LCT+TP	N15 (COR1) N11 (COR2)	E68±3 (COR1) E61±3 (COR2)		mean value of all points⋆
			CM+TP	N7 (COR1) N14 (COR2)	E65±3 (COR1) E66±3 (COR2)		mean value of all points⋆⋆
		Mierla et al. 2009	PR-A	N8 (COR1) N13 (COR2)	E72 (COR1) E53 (COR2)		mean value of all points⋆⋆
15 May 2007							
19:00	8		PR-B	N10 (COR1) N16 (COR2)	E74 (COR1) E64 (COR2)		mean value of all points⋆⋆
		Mierla et al. 2008	3D-HT	N6±0.5 (COR1)	E65±9 (COR1)	169	structure inside the CME⋆
		Temmer et al. 2009	TP-LE	N01±1 (COR1)	E48±2 (COR1)	445±11	LE; LASCO+ COR⋆
		Mierla et al. 2008	3D-HT	S30±1 (COR1)	W1±1 (COR1)	548	structure on LE⋆
05/20/2007	9						
06:00		Srivastava et al. (2009)	TP	S30 (COR1)	W15 (COR1)	510	structure on LE⋆⋆
		Srivastava (2009)	3D-HT	S30 (COR2)	W1.7 (COR2)	544	
		Boursier et al. 2009	FM-LE	S19 (COR2)	W120 (COR2)	502	LE
			TP-CoG	S14 (COR2)	W103 (COR2)	150	CM⋆⋆
21 Aug 2007 07:00 UT	26	de Koning et al. 2009	TP	S11±2 (beacon)	W124±4 (beacon)	373±6(LE) 274±12 (CM)	triang. of CM
		Moran et al. 2010	PR	S0 (COR1)	W147 (COR1)		filamentary material seen best from A
			TP	S0 (COR1)	W140 (COR1)		
		Temmer et al. 2009	TP-LE	S10±6	W120±3	403±15	LE; LASCO+ COR-A⋆
16 Nov 2007	40	Thernisien et al. (2009)	FM	S14	W123	345	flux-rope
05:45 UT		Howard and Tappin 2008	TP	S14	W73		LE central part relative to LASCO ⋆
		Liewer et al. (2009b)	TP+Tr	S13 (COR2)	W105 (COR2)	383	LE⋆
		Antunes et al. 2009	InvRec+	S12 (COR2)	E88 (COR2)	300	CM
			FM	S7 (COR2)	E88 (COR2)	800	LE
		Temmer et al. 2009	TP-LE	S15±0	E92±6	1002±11	LE; LASCO+ COR⋆
31 Dec 2007	44	Thernisien et al. (2009)	FM	S25 (COR2)	E80 (COR2)	972	LE
01:05 UT		Colaninno and Vourlidas 2009	MassConstr		E100 (COR2)		The same mass in A and B⋆⋆
		de Koning et al. 2009	TP	S31±6 (beacon)	E94±4 (beacon)	724±51(LE) 491±36 (CM)	triang. of the CM
		Liewer et al. (2009b)	TP-Tr	S23 (COR1+COR2)	E94 (COR1+COR2)	871	LE⋆

LASCO data to derive the propagation direction and speed of the leading edge of this CME. Two results were obtained by combining LASCO+STEREO A and LASCO+STEREO B images, which are then taken as the error estimation for the method (see Table 2). Note that the estimated longitude of 15 May 2007 CME as found by Temmer et al. (2009) differ by 20° from that obtained by Mierla et al. (2008) who used the 3D-HT method to determine the kinematic properties for a localized blob of plasma which could be identified within the CME cloud (Table 2).

Table 2. Continued.

Date	γ°	Author	Method	Lat	Lon	Speed km s^{-1}	Remarks
			LCT+TP	S15 (COR1) S2 (COR2)	E88±0.5 (COR1) E85±0.5 (COR2)		mean value of all points*
		Mierla et al. 2009	CM+TP	S14 (COR1) S7 (COR2)	E88±0.5 (COR1) E92±0.5 (COR2)		Mean value of all points**
			PR-A	S12 (COR1) S11 (COR2)	E58 (COR1) E50 (COR2)		mean value of all points**
25 Mar 2008 18:40 UT	47		PR-B	S14 (COR1) S7 (COR2)	E97 (COR1) E88 (COR2)		mean value of all points**
		Thernisien et al. (2009)	FM	S12 (COR2)	E84 (COR2)	1130	LE
		Temmer et al. 2009	TP-LE	S10±0	E82±7	1095±5	LE, LASCO+ COR*
		Colaninno and Vourlidas 2009	MassConstr		E78 (COR2)		the same mass in A and B**
		Maloney et al. 2009	TP	S33	E78	1020 (COR2) 478(+HI)	feature on LE*
		Liewer et al. (2009b)	TP-Tr	S9 (COR1+COR2)	E86 (COR1+COR2)	1087	LE*
		Thernisien et al. (2009)	FM	S13	E45	986	flux-rope
17 May 2008 10:25 UT	52	Wood et al. 2009	FM+ Kinem. model	S9	E48	959	

4.2 20 May 2007 CME

A partial halo CME associated with an eruptive filament was observed on 20 May 2007, 06:00 UT. The CME displayed a clear LE to the South of the Sun. The associated disk activity was recorded by the EUVI telescope. The spacecraft separation angle was ∼9°. Srivastava et al. (2009) have applied the TP method to reconstruct the LE in the COR1 and COR2 FOV. The LE observed in the coronagraph images and one tries to reconstruct is not necessarily the same LE that will arrive at Earth, since the LE is not unique. This is explained by the fact that the true leading edge of a CME is a three-dimensional feature. When it is observed from different viewpoints, it is projected on the plane of the sky in different ways. The image of the LE is thus not unique and depends on the location of the observer with respect to the CME. In particular, the part of the CME leading edge that is directed right towards the Earth cannot be imaged by an observer situated close to the Earth as the coronagraph occulter obstructs the imaging of this part of the CME. The authors obtained a reconstructed propagation speed for the LE of approximately 510 km s^{-1}, compared with the measured projected speeds of around 285 km s^{-1}. Their results compare well with the results of Mierla et al. (2008), who applied the 3D-HT technique to the same feature. Srivastava et al. (2009) also calculated the travel time to the Earth using their inferred 3-D speed which is in close agreement with the actual travel time and within the measurement errors.

4.3 21 August 2007 CME

The STEREO spacecraft separation angle on 21 August 2007 was 26°. Both spacecraft observed the CME at around 07:00 UT as a west-limb event. No obvious changes were observed in the SECCHI EUVI 19.5 nm images which would help identify the source region. Applying the geometric localization technique to this event, de Koning et al. (2009) obtained a HEEQ latitude and longitude of −11° and 124° respectively. They derived a speed of around 373 km s^{-1} for the LE, and a centroid speed of approximately 274 km s^{-1}. Boursier et al. (2009) obtained a LE speed of around 502 km s^{-1} and identified the center of gravity to be at S14, W103 (HEEQ coordinate system). Note that the difference of 20° obtained by the two methods is due to the larger uncertainties affecting the determination of CoG (Boursier et al., 2009). Also, the geometric localization technique has its limitation in characterizing the size and shape of the CMEs, when the spacecraft separation is less than 30° (de Koning et al., 2009). Moran et al. (2010), using the polarized ratio technique, estimated the position of the CME to be at ±57° ahead or behind the Sun-Earth POS, at west limb. The angle is given for the filamentary material seen best from COR-A. Taking into consideration the result of the TP technique the authors could establish that this was a back side event. The reconstructed parameters are different compared with those derived by the previous techniques. One possible reason for this discrepancy could be that different authors

reconstructed different features of the CME, (see the discussion in Sect. 5.2), as it was a complex CME with multiple bright fronts.

4.4 16 November 2007 CME

A south-west limb CME was observed on 16 November at around 05:45 UT when the separation angle of the two STEREO spacecraft was 40°. For this event, Howard and Tappin (2008) estimated the longitude of the central part of the LE as 73°. Temmer et al. (2009) using the triangulation method on COR and LASCO data obtained a longitude of 120°. They identified a particular feature on the LE that they could follow clearly in all spacecraft. Liewer et al. (2009b) obtained a longitude of 105° of the LE by using TP-Tr method. Thernisien et al. (2009) fitted a flux rope to the CME using FM technique and obtained an HEEQ longitude of 123°. The velocity derived for this event lies in the range of 350–400 km s^{-1}.

4.5 31 December 2007 CME

The CME was observed by both COR and LASCO as an east limb event at around 01:05 UT. The separation angle of the 2 STEREO spacecraft was 44°. This CME was nearly in the POS as seen from Earth. The front of this event appears to be strongly distorted in the COR2 FOV, and has a circular shape in the COR1 FOV. By applying different reconstruction techniques the longitude of this event was estimated to be −88° (LE) using the inverse reconstruction combined with FM (Antunes et al., 2009); −86° from triangulation of a feature on the LE (Temmer et al., 2009); −80° from the FM of Thernisien et al. (2009); −100° from mass constraints (Colaninno and Vourlidas, 2009); −94° from geometric localization technique (de Koning et al., 2009); −94° from tie-pointing plus triangulation of the LE (Liewer et al., 2009b).

4.6 25 March 2008 CME

This event was associated with a filament eruption, observed in EUVI 30.4 nm images. The neutral line of the source region was oriented in the east-west direction. The event is seen as a structured CME at the east limb in the COR1 images at around 18:40 UT. The separation angle of the two STEREO spacecraft was around 47°. The different reconstruction methods estimated longitude deviations up to 20°, except for the PR method which gives outliers up to 30°. These deviations may be due to the reason that the prominence material emission is measured in H_α and it is not due to Thomson scattering (e.g. Mierla et al., 2009). The true speeds measured in the COR2 FOV by the TP and FM techniques are ≈1100 km s^{-1} (Liewer et al., 2009b; Temmer et al., 2009; Thernisien et al., 2009; Maloney et al., 2009). Maloney et al. (2009) have extended their study to the HI FOV and they have derived a speed of 478 km s^{-1} including HI data, while the speed in COR2 was 1010 km s^{-1}. They have found in general that the CMEs slower than the solar wind were accelerated while the CMEs faster than the solar wind were decelerated (see e.g. Vršnak and Gopalswamy, 2002).

4.7 17 May 2008 CME

The separation of the STEREO spacecraft was 52° when a CME was recorded on 17 May 2008. At about 09:56 UT, the SECCHI/EUVI imagers on both spacecraft observed the beginning of a flare which also marked the initiation of the associated CME. The flare was observed close to the east limb in STEREO-A, but very close to disk center when viewed from STEREO-B. In EUVI-A He II 30.4 nm images, material was seen moving outward from the flare site following the flare. The event was observed as a full halo by COR2-B images, a partial halo by LASCO and as an east limb event by COR2-A. The CME appeared to have two separate fronts, particularly when viewed in HI1-A. Two bright fronts were observed, a narrow one was centered close to the ecliptic plane and a second faint broader front propagated northward from the source region (Wood et al., 2009). Using a FM and kinematic model they estimated a latitude and longitude of −9° and −48° for the CME LE. They estimated a true speed of 959 km s^{-1} in the COR2 FOV. Their results agree well with that of Thernisien et al. (2009) who obtained a latitude and longitude of −13° and −45° associated, and a 3-D speed of ≈986 km s^{-1}.

5 Error estimates

There are several sources of errors in the reconstruction of CMEs depending upon the technique used. The errors can be introduced by many factors, but these can largely be grouped into two main categories, observational and "methodical" errors. Observational errors include: different separation angles between the spacecraft; the shape and the orientation of the CME; and the propagation direction. Large errors appear when one tries to identify the same feature in A and B images. These occur typically for large separation angles when the two spacecraft see quite different parts of the CME. Methodical errors may come in the form of approximations and assumptions e.g.: radial propagation direction; self-similar expansion of CME etc. Another major contribution to the errors is when one tracks a LE which is the apparent LE seen from a given vantage point and may not be the LE as seen from the other vantage point. Moreover, the location of the apparent LE along a CME front can actually change as the CME expands outwards and the viewing angle changes.

An important source of error which is difficult to quantify comes from the fact that CMEs are optically thin objects. Different LOSs will cross different regions and the radiance integral for each line will further be differentially weighted by the amount of scattering from the feature along the line of sight. While a strict stereo reconstruction will benefit from

increasing separation angles, the above effect will, on the contrary, worsen due to misidentification of similar features.

5.1 Error estimates for each technique

For the tie-point technique the geometrical reconstruction errors depend on the base angle γ between the two STEREO spacecraft. For a point in a given epipolar plane and a pointing error of ds along the epipolar line in both images, the error in the depth estimate is $ds/\sin(\gamma/2)$. This implies that for large separation angles the errors are small. In such cases as we have mentioned above, the identification of similar objects in the pair of images is more difficult. In Mierla et al. (2009), the errors for the longitude in the case of LCT-TP and CM-TP methods are estimated using a pointing error along the epipolar lines of 1 pixel. The depth errors ($\mathrm{depth_{err}}$) were converted to longitude errors by $\mathrm{atan}(\mathrm{depth_{err}}/R_{\mathrm{CME}})$, where R_{CME} is the distance of the object from the Sun center. They obtained an error of 3° in longitude for 15 May 2007 CME (separation angle 8°) and 0.5° for the 25 March 2008 CME (separation angle 47°). Mierla et al. (2008) used 3D-HT technique to derive the direction of propagation and the un-projected speed of well localized plasma features inside the CME. The errors were calculated from the initially estimated errors resulting due to uncertainties in selecting the tracked objects: 1° (i.e., three pixels at 1.4 $R_{\odot}$ and nine pixels at 4 $R_{\odot}$) in azimuthal direction and 0.038 $R_{\odot}$ (5 pixels) in radial direction for COR1 FOV. They obtained an uncertainty of 9° and 1° in longitude for the CMEs of 15 May 2007 and 20 May 2007 respectively, while for the latitude the uncertainties were around 0.5° and 1°. Note that the CME on 15 May 2007 was a structured, east limb event, while the CME on 20 May 2007 was a partial halo CME seen mostly at the southern part of images.

Temmer et al. (2009) also included LASCO observations for their analysis. Combining LASCO + STEREO-A and LASCO + STEREO-B two results were obtained for each event they studied and used for error estimation. For most of the events, the results are consistent within 10° in longitude and latitude. The 22 January 2008 case is an exception with a difference of 20° in longitude and more than 40° in latitude. This variation is related to the fact that STEREO-A observes this event as a partial halo. The spacecraft which observes the CME moving close to its line of sight cannot track corresponding features observed by the other spacecraft. Furthermore, the assumption of the radial outward motion of the CME might be unjustified for some of the events (this might be the case for the differences for the 16 November 2007 event – cf. Temmer et al., 2009).

Howard and Tappin (2008) separated the relative location of the leading edge of a CME in the northern and southern flanks and the central location and assumed that these were the same location in the projected image of each observer. They then simply applied geometry to triangulate the location of each, and identified the 3-D location of two events near the solar limb. It was found that the most accurate measurements were those made furthest from the equatorial plane, since the three spacecraft (the twin STEREO and SOHO) orbit here. When the spacecraft and the measured point are co-planar, large deviations affect the results even if measurements errors are relatively small. Simulations suggest that geometric localization works best when the spacecraft separation is greater than 30° and less than 150° (de Koning et al., 2009).

Thernisien et al. (2009) have estimated the errors for their flux-rope like model using a sensitivity analysis method. Basically, for each CME the authors vary one parameter at a time, in both the positive and negative direction around the maximum of the merit function until it decreases to 10% of the maximum value of that merit function. The range of variation gives an estimate of the precision. For the 26 events studied they found a mean value of $\pm 4.3°$ (with a maximum value of 16.6°) in longitude, and $\pm 1.8°$ (max value of 3.7°) in latitude. The best FM results are achieved when the CME looks very different from the two viewpoints, e.g. if the CME is seen as a halo in one spacecraft and as a limb event in the other spacecraft (Wood et al., 2009). This is not the case for the mass constraint technique (Colaninno and Vourlidas, 2009), since a portion of the CME is behind the occulter and their assumption that they are observing the same mass in both views is not valid. For the MassConstr technique the error in the CME direction arises from the shape of the mass function with POS angle. When considering small spacecraft separations, small differences between the two masses can cause large differences in the direction. Assuming a typical mass error estimate of $\sim$15, and a spacecraft separation larger than 50° the direction ambiguity becomes reasonably small ($\lesssim$20°) (Colaninno and Vourlidas, 2009).

5.2 Error estimates from applying the techniques to common events

All the results presented in Table 2 agree well, and are within about 10° of each other, with some exceptions. Some of these exceptions are due to the fact that different techniques were applied to different parts of the CME. Temmer et al. (2009) tracked common features (such as density variations or prominently shaped structures) close to the central part of the leading edge, along the main propagation direction. Mierla et al. (2008) followed compact plasma blobs which could be identified in a CME cloud. Howard and Tappin (2008) identified a feature near the center of the LE that was present in all three spacecraft images. Thernisien et al. (2009), using a flux-rope like model tried to fit the peak of brightness on the leading edge, which corresponds to the peak of electron density in the skin or shell of the model. Boursier et al. (2009) approximated the LE by a spherical shell, and then calculated the position of the farthest point of the LE from the center of the Sun. These points were tracked with time for estimating the speeds. Boursier et al.

(2009); Colaninno and Vourlidas (2009); de Koning et al. (2009) tracked the direction of propagation of the center of mass of the CME.

6 Discussions and conclusions

Space weather forecasters need to determine accurately whether a CME is Earth directed, and, if so, when it would impact the Earth. For practical applications, it is important that a forecast is made well before a CME arrives at the Earth. Forecasters are less concerned with the fine structure of CMEs, although it is helpful to gain a general picture of its overall shape. Table 2 shows that all the reconstruction techniques give a good estimate of the gross properties of CMEs, such as the CME location, speed, and direction of propagation, with an exception of a few outliers. In general, the propagation angles obtained using different techniques were within $\sim 10^{\circ}$.

The propagation direction of a CME differed by up to 20° in longitude from that of its source region on the solar disk. It does not seem improbable that the CMEs may be deflected (e.g. St. Cyr et al., 1999) by more than 10° when they are still close to the solar surface.

Another interesting aspect is the relationship between the CME and the flaring region. The question is whether the CME source region is always the same as the associated flare region. We know that there are well observed CMEs without any flare brightening (e.g. Munro et al., 1979; Howard and Tappin, 2008). It seems that faster CMEs are located closer to the on-disk flare region than the slower ones (e.g. MacQueen, 1980; Yashiro et al., 2008). A similar result is obtained by Temmer et al. (2009).

Another important aspect for forecasters is the magnetic field configuration of the CME source region, and its in situ consequences, essentially its geoeffectiveness. The B_z orientation of the CME is of particular interest and it would be valuable to identify this from the magnetic field structure on the Sun. It might be possible to get such information, if the full 3-D shape of the CME material (core plus LE – see Fig. 1) can be reconstructed. The reconstruction of the shape of the CME core will give information about the magnetic field orientation of the filament. And, as we pointed out in the introduction section, the magnetic field orientations of the filaments on the solar disk and of the associated magnetic clouds are sometimes closely related.

To summarize, the reconstruction techniques presented here estimate the most probable CME propagation direction at the outer boundary of the corona (observed in coronagraph images) to within $\sim 10^{\circ}$. Not all methods work equally well for limb (from Earth) events.

There are several limitations to each technique as applied to the data which need to be overcome. Additional parameters like the density extremes within the CME needs to be explored. Additional observations from a third view direction close to the Earth (SMEI, MK IV, LASCO) would be valuable for 3-D reconstructions, particularly when the STEREO spacecraft attain larger separation angles.

Acknowledgements. M. M. would like to thank SIDC and ROB for the financial support and for the facilities to carry out this work. M. T. is a recipient of an APART-fellowship of the Austrian Academy of Sciences at the Institute of Physics, University of Graz (APART 11262). We acknowledge the SECCHI/STEREO and SOHO/LASCO consortia for providing the data. The SECCHI data used here were produced by an international consortium of the Naval Research Laboratory (USA), Lockheed Martin Solar and Astrophysics Lab (USA), NASA Goddard Space Flight Center (USA), Rutherford Appleton Laboratory (UK), University of Birmingham (UK), Max-Planck Institute for Solar System Research (Germany), Centre Spatiale de Liège (Belgium), Institut d'Optique Théorique et Appliquée (France), Institut d'Astrophysique Spatiale (France). The LASCO data used here were produced by an international consortium of the Naval Research Laboratory (USA), the Laboratoire d'Astrophysique de Marseille (France, the former Laboratoire d'Astronomie Spatiale), the Max-Planck Institute for Solar System Research (Germany), and the School of Physics and Astronomy, University of Birmingham, (UK). SoHO is a project of joint collaboration by ESA and NASA.

Topical Editor R. Forsyth thanks B. Jackson and Y. Li for their help in evaluating this paper.

References

Antunes, A., Thernisien, A., and Yahil, A.: Hybrid Reconstruction to Derive 3D Height-Time Evolution for Coronal Mass Ejections, Solar. Phys., 259, 199–212, 2009.

Aschwanden, M. J., Burlaga, L. F., Kaiser, M. L., Ng, C. K., Reames, D. V., Reiner, M. J., et al.: Theoretical modeling for the stereo mission, Space Sci. Rev., 136, 565–604, 2008.

Billings, D. E.: A guide to the Solar Corona, Academic Press, NY, London, 1966.

Boursier, Y., Lamy, P., and Llebaria, A.: Three-Dimensional Kinematics of Coronal Mass Ejections from STEREO/SECCHI-COR2 Observations in 2007–2008, Solar Phys., 256, 131–147, 2009.

Boursier, Y. and Lamy, P.: Forward modeling of the 23 October 2003 CME by an assymetric model, Solar Phys., to be submitted, 2010.

Brueckner, G. E., Howard, R. A., Koomen, M. J., Korendyke, C. M., Michels, D. J., Moses, J. D., et al.: The Large Angle Spectroscopic Coronagraph (LASCO), Solar Phys., 162, 357–402, 1995.

Chen, J., Howard, R. A., Brueckner, G. E., Santoro, R., Krall, J., Paswaters, S. E., St. Cyr, O. C., Schwenn, R., Lamy, P., and Simnett, G. M.: Evidence of an Erupting Magnetic Flux Rope: LASCO Coronal Mass Ejection of 1997 April 13, Astrophys. J., 490, L191, doi:10.1086/311029, 1997.

Chen, J., Santoro, R. A., Krall, J., Howard, R. A., Duffin, R., Moses, J. D., Brueckner, G. E., Darnell, J. A., and Burkepile, J. T.: Magnetic Geometry and Dynamics of the Fast Coronal Mass Ejection of 1997 September 9, Astrophys. J., 533, 481–500, 2000.

Colaninno, R. and Vourlidas, A.: First Determination of the True Mass of Coronal Mass Ejections: A Novel Approach to Using the Two STEREO Viewpoints, Astrophys. J., 698, 852–858, 2009.

Cremades, H. and Bothmer, V.: On the three-dimensional configuration of coronal mass ejections, Astron. Astrophys. 422, 307–322, 2004.

de Koning, C. A., Pizzo, V. J., and Biesecker, D. A.: Geometric Localization of CMEs in 3D Space Using STEREO Beacon Data: First Results, Solar Phys., 256, 167–181, 2009.

Dere, K. P., Wang, D., and Howard, R.: Three-dimensional Structure of Coronal Mass Ejections from LASCO Polarization Measurements, Astrophys. J., 620, L119–L122, 2005.

Feng, L., Inhester, B., Solanki, S., Wiegelmann, T., Podlipnik, B., Howard, R. A., and Wuelser, J.-P.: First Stereoscopic Coronal Loop Reconstructions from STEREO SECCHI Images, Astrophys. J. 671, L205–L208, 2007.

Gibson, S. E. and Low, B. C.: A Time-Dependent Three-Dimensional Magnetohydrodynamic Model of the Coronal Mass Ejection, Astrophys. J., 493, 460–473, 1998.

Gonzalez, W. D. and Tsurutani, B. T.: Criteria of interplanetary parameters causing intense magnetic storms (Dst of less than −100 nT), Planet. Space Sci., 35, 1101–1109, 1987.

Gopalswamy, N., Yashiro, S., Xie, H., Akiyama, S., and Makela, P.: Large Geomagnetic Storms Associated with Limb Halo Coronal Mass Ejections, eprint arXiv:0903.2776, Adv. Geosci., accepted, 2010.

Gosling, J. T., Bame, S. J., McComas, D. J., and Phillips, J. L.: Coronal mass ejections and large geomagnetic storms, Geophys. Res. Lett., 17, 901–904, 1990.

Howard, R. A., Moses, J. D., Vourlidas, A., Newmark, J. S., Socker, D. G., Plunkett, S. P., et al.: Sun Earth Connection Coronal and Heliospheric Investigation (SECCHI), Space Sci. Rev., 136, 67–115, 2008.

Howard, T. A. and Tappin, S. J.: Three-dimensional reconstruction of two solar coronal mass ejections using the STEREO spacecraft, Solar Phys., 252, 373–383, 2008.

Illing, R. M. E. and Hundhausen, A. J.: Disruption of a coronal streamer by an eruptive prominence and coronal mass ejection, J. Geophys. Res., 91, 10951–10960, 1986.

Inhester, B.: Stereoscopy basics for the STEREO mission, to appear as a Publ. of the Int. Space Sci. Inst., astro-ph/0612649, 2006.

Jackson, J. D.: Classical Electrodynamics (3rd ed.; New York: Wiley), 1997.

Jackson, B. V. and Hick, P. P.: Chapter 17 in: Solar and Space Weather Radiophysics, Current Status and Future Developments, edited by: Gary, D. E., and Keller, C. U., Astrophysics and Space Science Library 314, p. 355-386, Kluwer Academic Publ., Dordrecht, The Netherlands, 2005.

Jackson, B. V., Buffington, A., Hick, P. P., Wang, X., and Webb, D.: Preliminary three-dimensional analysis of the heliospheric response to the 28 October 2003 CME using SMEI white-light observations, J. Geophys. Res., 111, A04S91, doi:10.1029/2004JA010942, 2006.

Jackson, B. V., Bisi, M. M., Hick, P. P., Buffington, A., Clover, J. M., and Sun, W.: Solar Mass Ejection Imager 3-D reconstruction of the 27-28 May 2003 coronal mass ejection sequence, J. Geophys Res., 113, A00A15, doi:10.1029/2008JA013224, 2008.

Kaiser, M. L., Kucera, T. A., Davila, J. M., St. Cyr, O. C., Guhathakurta, M., and Christian, E.: The STEREO Mission: An Introduction, Space Sci. Rev., 136, 5–16, 2008.

Krall, J. and St.Cyr, O. C.: Flux-Rope Coronal Mass Ejection Geometry and Its Relation to Observed Morphology, Astrophys. J., 652, 1740–1746, 2006.

Krall, J., Yurchyshyn, V. B., Slinker, S., Skoug, R. M., and Chen, J.: Flux Rope Model of the 2003 October 28-30 Coronal Mass Ejection and Interplanetary Coronal Mass Ejection, Astrophys. J., 642, 541–553, 2006.

Krall, J.: Are All Coronal Mass Ejections Hollow Flux Ropes?, Astrophys. J., 657, 559–566, 2007.

Liewer, P. C., De Jong, E. M., Hall, J. R., Howard, R. A., Thompson, W. T., Culhane, J. L., Bone, L., and van Driel-Gesztelyi, L.: Stereoscopic Analysis of the 19 May 2007 Erupting Filament, Solar Phys., 256, 57–72, 2009a.

Liewer, P. C., De Jong, E. M., Hall, J. R., Howard, R. A., Sheeley, N., and Thompson, W. T.: Solar Wind 12, AIP, 2009b.

MacQueen, R. M.:Coronal transients – A summary, Phil. Trans. R. Soc. Lond., 297, 605–620, 1980.

Maloney, S. A., Gallagher, P. T., and McAteer, R. T. J.: Reconstructing the 3-D Trajectories of CMEs in the Inner Heliosphere, Solar Phys., 256, 149–166, 2009.

Manchester, W. B., Gombosi, T. I., Roussev, I., De Zeeuw, D. L., Sokolov, I. V., Powell, K. G., Tóth, G., and Opher, M.: Three-dimensional MHD simulation of a flux rope driven CME, J. Geophys. Res., 109, A01102, doi:10.1029/2002JA009672, 2004.

Michalek, G., Gopalswamy, N., and Yashiro, S.: A New Method for Estimating Widths, Velocities, and Source Location of Halo Coronal Mass Ejections, Astrophys. J., 584, 472–478, 2003.

Michalek, G.: An Asymmetric Cone Model for Halo Coronal Mass Ejections, Solar Phys., 237, 101–118, 2006.

Mierla, M., Davila, J., Thompson, W., Inhester, B., Srivastava, N., Kramar, M., StCyr, O. C., Stenborg, G., and Howard, R. A.: A Quick Method for Estimating the Propagation Direction of Coronal Mass Ejections using STEREO-COR1 Images, Solar Phys., 252, 385–396, 2008.

Mierla, M., Inhester, B., Marque, C., Rodriguez, L., Gissot, S., Zhukov, A., Berghmans, D., and Davila, J.: On 3D Reconstruction of Coronal Mass Ejections: I Method description and application to SECCHI-COR Data, Solar Phys., 259, 123–141, 2009.

Minnaert, M.: On the continuous spectrum of the corona and its polarisation. With 3 figures. (Received July 30, 1930), Z. Astrophys. 1, 209–236, 1930.

Moran, T. G. and Davila, J. M.: Three-Dimensional Polarimetric Imaging of Coronal Mass Ejections, Science, 305, 66–71, 2004.

Moran, T. G., Davila, J. M., and Thompson, W. T.: Three-dimensional Coronal Mass Ejection Structure and Orientation from Polarimetric and Geometric Analyses of Stereoscopic Observations, Astrophys. J., submitted, 2010.

Munro, R. H.: Coronal transients: arches or bubbles?, Topical Conference on Solar and Interplanetary Physics, Tucson, Arizona, January 12–15, 10, 1977.

Munro, R. H., Gosling, J. T., MacQueen, R. M., Poland, A. I., and Ross, C. L.: The association of coronal mass ejection transients with other forms of solar activity, Solar Phys., 61, 201–215, 1979.

Pizzo, V. J. and Biesecker, D. A.: Geometric localization of STEREO CMEs, Geophys. Res. Lett., 31, L21802, doi:10.1029/2004GL021141, 2004.

Puetter, R. C., Gosnell, T. R., and Yahil, A.: Digital Image Reconstruction: Deblurring and Denoising, Ann. Rev. Astr. Astrophys. Suppl., 43, 139–194, 2005.

Rodriguez, L., Zhukov, A. N., Gissot, S., and Mierla, M.: Three-

Dimensional Reconstruction of Active Regions, Solar Phys., 256, 41–55, 2009.

Russell, C. T., McPherron, R. L., and Burton, R. K.: On the cause of geomagnetic storms., J. Geophys. Res., 79, 1105–1109, 1974.

Ruzmaikin, A., Martin, S. F., and Hu. Q., J.: Signs of magnetichelicity in interplanetary coronal mass ejections and associated prominences: Case study, Geophys. Res., 108, 1096, doi:10.1029/2002JA009588, 2003.

Schwenn, R., Dal Lago, A., Huttunen, E., and Gonzalez, W. D.: The association of coronal mass ejections with their effects near the Earth, Ann. Geophys., 23, 1033–1059, 2005, http://www.ann-geophys.net/23/1033/2005/.

Srivastava, N. and Venkatakrishnan, P.: Relationship between CME Speed and Geomagnetic Storm Intensity, Geophys. Res. Lett., 29, 1287, doi:10.10292001GL013597, 2002.

Srivastava, N. and Venkatakrishnan, P.: Solar and interplanetary sources of major geomagnetic storms during 1996–2002, J. Geophys. Res., 109, A010103, doi:10.1029/2003JA010175, 2004.

Srivastava, N.: CME observations from STEREO, Astrophysics and Space Science Proceedings) series, Proc. of the Evershed meeting, Springer, edited by: Hasan, S. S. and Rutten, R., 2009.

Srivastava, N., Inhester, B., Mierla, M., and Podlipnik, B.: 3D Reconstruction of the Leading Edge of the May 20, 2007 Partial Halo CME, Solar Phys., 259, 213–225, 2009.

St. Cyr, O. C., Burkepile, J. T., Hundhausen, A. J., and Lecinski, A. R.: A comparison of ground-based and spacecraft observations of coronal mass ejections from 1980–1989, J. Geophys. Res., 104, 12493–12506, 1999.

Tappin, S. J. and Howard, T. A.: Interplanetary Coronal Mass Ejections Observed in the Heliosphere: 2. Model and Data Comparison, Space Sci. Rev., 147, 55–87, doi:10.1007/s11214-009-9550-5, 2009.

Temmer, M., Preiss, S., and Veronig, A. M.: CME projection effects studied with STEREO/COR and SOHO/LASCO, Solar Phys., 256, 183–199, 2009.

Thernisien, A. F. R., Howard, R. A., and Vourlidas, A.: Modeling of Flux Rope Coronal Mass Ejections, Astrophys. J., 652, 763–773, 2006.

Thernisien, A., Vourlidas, A., and Howard, R. A.: Forward Modelling of Coronal Mass Ejections using STEREO-SECCHI Data, Solar Phys., 256, 111–130, 2009.

Thompson, W. T., Davila, J. M., Fisher, R. R., Orwig, L. E., Mentzell, J. E., Hetherington, S. E., et al.: COR1 inner coronagraph for STEREO-SECCHI, in: Innovative Telescopes and Instrumentation for Solar Astrophysics, edited by: Keil, S. L. and Avakyan, S. V., Proc. SPIE 4853, 1–11, 2003.

Thompson, W. T.: Coordinate systems for solar image data, A&A, 449, 791–803, 2006.

Thompson, W. T. and Reginald, N. L.: The Radiometric and Pointing Calibration of SECCHI COR1 on STEREO, Solar Phys., 250, 443–454, 2008.

Tokumaru, M., Kojima, M., Fujiki, K., Yamashita, M., and Jackson, B. V.: The source and propagation of the interplanetary disturbance associated with the full-halo coronal mass ejection on 28 October 2003, J. Geophys. Res., 112, A05106, doi:10.1029/2006JA012043, 2007.

Trucco, E. and Verri, A.: Introductory Techniques for 3-D Computer Vision, Prentice Hall, New Jersey, 1998.

Van de Hulst, H. C.: The electron density of the solar corona, B. Astron. Inst. Netherlands, 11, 135–150, 1950.

Vršnak, B. and Gopalswamy, N.: Influence of the aerodynamic drag on the motion of interplanetary ejecta, J. Geophys. Res., 107, 1019, doi:10.1029/2001JA000120, 2002.

Vršnak, B., Sudar, D., Ruždjak, D., and Žic, T.: Projection effects in coronal mass ejections, Astron. Astrophys., 469, 339–346, 2007.

Wood, B. E., Howard, R. A., Thernisien, A., Plunkett, S. P., and Socker, D. G.: Reconstructing the 3D Morphology of the 2008 May 17 CME, Solar Phys., 259, 163–178, 2009.

Wu, S. T., Andrews, M. D., and Plunkett, S. P.: Numerical Magnetohydrodynamic (MHD) Modeling of Coronal Mass Ejections (CMEs), Space Sci. Rev., 95, 191–213, 2001.

Xie, H., Ofman, L., and Lawrence, G.: Cone model for halo CMEs: Application to space weather forecasting, J. Geophys. Res., 109, A03109, doi:10.1029/2004JA010501, 2004.

Yashiro, S., Michalek, G., Akiyama, S., Gopalswamy, N., and Howard, R. A.: Spatial Relationship between Solar Flares and Coronal Mass Ejections, Astrophys. J., 673, 1174–1180, 2008.

Yurchyshyn, V., Wang, H., and Abramenko, V.: How directions and helicity of erupted solar magnetic fields define geoeffectiveness of coronal mass ejections, Adv. Space Res., 32, 1965–1970, 2003.

Yurchyshyn, V., Yashiro, S., Abramenko, V., Wang, H., and Gopalswamy, N.: Statistical Distributions of Speeds of Coronal Mass Ejections, Astrophys. J., 619, 599–603, 2005.

Zhao, X. P., Plunkett, S. P., and Liu, W.: Determination of geometrical and kinematical properties of halo coronal mass ejections using the cone model, J. Geophys. Res., 107, 1223, doi:10.1029/2001JA009143, 2002.